ISSN 1063-780X, Plasma Physics Reports, 2020, Vol. 46, No. 4, pp. 363–373. © Pleiades Publishing, Ltd., 2020.
Published in Russian in Fizika Plazmy, 2020, Vol. 46, No. 4, pp. 318–328.

PLASMA DYNAMICS

Stability of Ion Flow and Role of Boundary Conditions in a Simplified Model of the E × B Plasma Accelerator with a Uniform Electron Mobility

I. V. Romadanov[a, *], A. I. Smolyakov[a, b], E. A. Sorokina[b, c], V. V. Andreev[b], and N. A. Marusov[b, c]

[a] *Department of Physics and Engineering Physics, University of Saskatchewan, Saskatoon, SK S7N 5E2 Canada*

[b] *Peoples' Friendship University of Russia (RUDN University), Moscow, 117198 Russia*

[c] *NRC "Kurchatov Institute," Moscow, 123182 Russia*

**e-mail: ivr509@mail.usask.ca*

Received September 12, 2019; revised November 20, 2019; accepted November 21, 2019

Abstract—Resistive oscillations of axial plasma with ionization effects are analyzed in configuration similar to the Hall effect thrusters. From analysis of stationary equations we have identified different types of the steady-state plasma flow profiles and use these solutions as initial conditions in time-dependent initial value simulations. We have identified unstable regimes with intrinsic oscillations, as well as stable regions without oscillations. It was found that nonlinear oscillations may exist in different form depending on the range of plasma parameters. Single mode coherent, multi-mode with nonlinear harmonics, and incoherent (stochastic) mode regimes were identified. We have further investigated the role of boundary conditions on the characteristics of nonlinear oscillations.

Keywords: plasma in crossed fields, axial oscillations, pulsed mode, nonlinear modeling, stationary plasma flows

DOI: 10.1134/S1063780X20040108

1. INTRODUCTION

Plasma flows are typical for a large class of plasma devices including plasma sources and accelerators, magnetrons and MHD plasma generators [1–7]. Acceleration of partially magnetized plasma is a basis for space propulsion systems and magnetrons where the magnetized electrons are confined by relatively strong magnetic field while unmagnetized ions can be accelerated by the electric field perpendicular to the magnetic field. Such systems are prone to a variety of instabilities which affect discharge operation and efficiency but are not well understood and remains a subject of active theoretical and experimental studies. One example is Hall Effect Thrusters (HET) for electric propulsion in space [8–11]. In this paper we consider the nonlinear dynamics of the axial modes (in the direction of the applied electric field). Such an instability is closely related to the well known breathing mode in Hall thrusters [8, 12]. Similar instability also exists in magnetron systems [4]. Despite long history of studies, there is no uniformly accepted model and clear understanding of the conditions for this instability. It is generally agreed that ionization is crucial for this mode, and very basic model was proposed based on the competition of the ionization and ion and neutrals flow [13–15]. This model only involves ion and neutrals with constant velocities, and no self consistent evolution of the electric field is involved. The other authors have argued that electron dynamics [16–21] and temperature fluctuations [22]; for an overview of the recent work see [23].

Acceleration of quasineutral plasma involves the singularity at the sonic point where the ion velocity is equal to the local ion sound velocity. Removal of singularity is important for the construction of smooth solutions and was analysed in [24–26]. It was shown recently [27] that regularization of the sonic point can be done analytically, revealing the existence of global constraints on stationary solutions. These constraints define the parameters in the operational space diagram for existence of stationary solutions. Different types of steady-state solutions were found [27] depending on the discharge current and neutral gas injection rate. It was hypothesized that different types of stationary solutions may have different stability properties and different characteristics of nonlinear oscillations (in unstable cases).

The focus of this work is a study of stability and nature of low frequency axial oscillations for conditions with different types of stationary solutions. We use the steady-state profiles that were obtained from the solution of stationary one-dimensional equations and study their time evolution in the initial value nonlinear simulations. We show here that low-frequency

modes may exist in different regimes such as single mode, highly coherent oscillations, as well as multi-mode regimes involving several modes.

The presence of the regularized sonic point makes stationary plasma profiles rather stiff due to global constraints imposed at the sonic point. Therefore one can expect that boundary conditions may affect the stability and nature of fluctuations. We investigate the effect of boundary conditions on the low frequency oscillations, in particular, the role of the ion velocity and plasma density boundary values at the anode.

In our work, we make a simplifying assumption that the electron mobility is constant and uniform. Typically, in such system, the electron mobility is highly anomalous. The profiles of the anomalous mobility are not well known [28] and the level of anomality (deviation from the classical values) is typically largest in the near-anode region [28, 29]. Assumptions of the constant classical mobility and constant ionization frequency, though not fully realistic for practical Hall thrusters, may be most appropriate for modified near-anode region of Hall thrusters. We comment on the role of the magnitude of the mobility on our results in the Summary section.

This paper is organized as follow. In Section 2 a brief description of the model and simulation parameters are given. Section 3 discusses the structure of stationary solutions and operational space diagrams. In Section 4 the results of stability studies for obtained steady-state solutions are presented. Effects of boundary conditions (BC) on the stability and oscillations are considered in Section 5. Summary and conclusions are given in Section 6.

2. BASIC PHYSICS MODEL FOR PLASMA ACCELERATION IN PRESENCE OF AXIAL IONIZATION AND RESISTIVITY

A basic model includes continuity equations for plasma $n(x,t)$ and neutral $N(x,t)$ densities, the ion momentum $v_i(x,t)$ equation, and the electric field E (obtained from the Ohm's law)

$$\frac{\partial N}{\partial t} + v_a \frac{\partial N}{\partial x} = -\beta N n, \tag{1a}$$

$$\frac{\partial n}{\partial t} + \frac{\partial}{\partial x}(n v_i) = \beta N n, \tag{1b}$$

$$\frac{\partial v_i}{\partial t} + v_i \frac{\partial v_i}{\partial x} = \frac{e}{m_i} E + \beta N (v_a - v_i), \tag{1c}$$

$$E = \frac{J_d}{n\mu_e} - \frac{v_i}{\mu_e} - \frac{1}{en}\frac{\partial (T_e n)}{\partial x}, \tag{1d}$$

where β is the ionization rate, m_i is the mass of ions, v_a is the neutral flow velocity, $J_d = n(v_i - v_e)$ is the discharge current flux, v_e is the velocity of electrons, μ_e is the electron mobility perpendicular to the magnetic field, T_e is the electron temperature, e is the elementary charge, and x defines the direction along the channel axis. These equations imply quasi-neutrality: $n_i = n_e = n$. The ionization is included in Eqs. (1a), (1b) with the constant velocity of neutral atoms v_a, injected from the anode side and assuming a simplest case of constant electron temperature [30, 31], so that ionization coefficient $\beta = \text{const}$.

Table 1. Typical plasma parameters in CHT

Parameter	Value
Gas	Xe
Channel length, L	3.0 cm
Channel radius, R	1.2 cm
Channel area, S	4.5 cm^2
Mass flow, $\dot{m}$	0.34 mg/s
Electron temperature, T_e	20 eV
Ion sound, c_s	3833 m/s
Neutral velocity, v_a	202 m/s ($T = 650$ K)
Electron mobility, μ_e	2.66 m^2/V s

The diffusion term $(en)^{-1}\partial(T_e n)/\partial x$ in Ohm's law results in the backward plasma flow to the anode (presheath region), and also leads to a singularity at the sonic point, $v_i = c_s$, where $c_s^2 = T_e/m_i$ is the ion sound velocity. The neutral velocity is assumed constant, $v_a = \text{const}$, and ions are assumed to be cold. As noted in the Introduction, we assume that the electron mobility μ_e is constant and uniform. Plasma parameters typical for the cylindrical Hall thruster (CHT) [32–34] were used in simulations. Electron temperature T_e was taken constant along the channel, what implies that the ionization rate coefficient $\beta = 1.29\times10^{-13}$ is constant as well. All parameters are summarized in the Table 1.

3. STATIONARY SOLUTIONS

Solutions of stationary equations for accelerating plasma flow were considered previously [24, 35]. Here we present a semi-analytical approach from a model in [27]. Setting all time derivatives to zero in (1) one has

$$v_a \frac{\partial N}{\partial x} = -\beta N n_i, \tag{2a}$$

$$\frac{\partial}{\partial x}(n_i v_i) = \beta N n_i, \tag{2b}$$

$$v_i \frac{\partial v_i}{\partial x} = -\frac{e}{m_i}\frac{\partial \phi}{\partial x} + \beta N (v_a - v_i), \tag{2c}$$

$$\frac{\partial \phi}{\partial x} = -\frac{J_d}{n_i \mu_e} + \frac{v_i}{\mu_e} + \frac{1}{en_i}\frac{\partial (T_e n_i)}{\partial x}, \tag{2d}$$

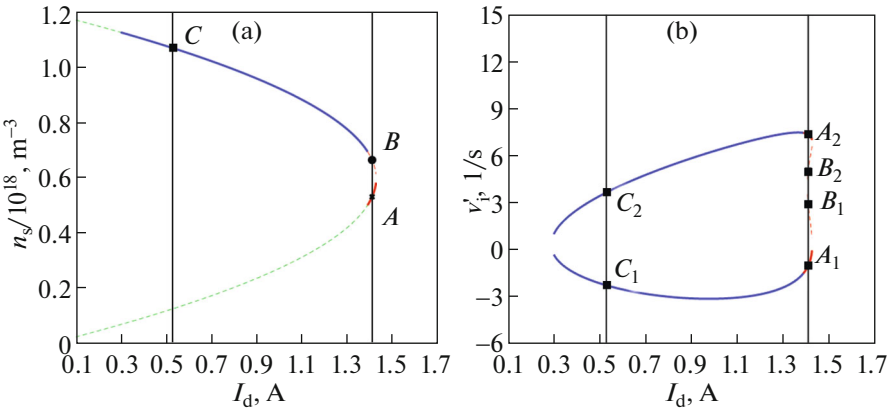

Fig. 1. Diagrams of (a) n_s and (b) v_i' as functions of the discharge current I_d at fixed value of J_a. Three n_s roots A, B, and C were chosen to illustrate different solutions.

where ϕ is the electrostatic potential, $E = -\partial\phi/\partial x$. The neutral's flux is defined as $J_a = Nv_a$ and the following integral is conserved $J_a + n_i v_i = \text{const}$. The neutral density at the boundary N can be found taking into account the ion recycling at the anode: the back flow ions driven to the anode are neutralised and added to the neutral injection flux, $N = \dot{m}/(m_i v_a S) - n_i v_i / v_a$, where S is a thruster channel cross-section. The system of equations (1) can be further transformed into a set of three ordinary differential equations for derivatives of v_i, n_i, and ϕ, which are written as follows

$$v_i' = -\frac{1}{c_s^2 - v_i^2}\left(v_i \frac{e}{m_i}\frac{J_d - n_i v_i}{\mu_e n_i} - \frac{J_a - n_i v_i}{v_a}\beta(c_s^2 + v_i^2 - v_a v_i)\right) \equiv \frac{F_1(v_i, n_i)}{D}, \quad (3a)$$

$$n_i' = \frac{1}{c_s^2 - v_i^2}\left(\frac{e}{m_i}\frac{J_d - n_i v_i}{\mu_e} + \frac{J_a - n_i v_i}{v_a}\beta n_i (v_a - 2v_i)\right) \equiv \frac{F_2(v_i, n_i)}{D}, \quad (3b)$$

$$\phi' = \frac{1}{c_s^2 - v_i^2}\left(v_i^2 \frac{J_d - n_i v_i}{\mu_e n_i} + \frac{m_i}{e}\frac{J_a - n_i v_i}{v_a}\beta c_s^2 (v_a - 2v_i)\right) \equiv \frac{F_3(v_i, n_i)}{D}, \quad (3c)$$

where $\phi' = \partial\phi/\partial x$, $v_i' = \partial v_i/\partial x$, $n_i' = \partial n_i/\partial x$, and $D = c_s^2 - v_i^2$. The right-hand side of this system depends on two parameters J_d and J_a as well as the running values of n_i and v_i. In case of the uniform electron temperature, the value of v_i is known at the singular point $v_i = c_s$ at $x = x_s$. Thus, equations (3a)–(3c) can be integrated from the sonic point (in both directions) if density is known at this point, $n_s = n_i(x_s)$. It turns out that for uniform fixed temperature the value n_s can be easily found from the regularity condition at the sonic point $x = x_s$, which is written in the form $F_1 = F_2 = F_3 = 0$, thus removing the singularity at the sonic point. It is important to note that equations for all three functions $F_1 = 0$, $F_2 = 0$, and $F_3 = 0$ reduce to a single equation

$$\beta\mu_e c_s (v_a - 2c_s) n_s^2 + (c_s v_a + \beta\mu_e J_a (2c_s - v_a)) n_s - J_d v_a = 0. \quad (4)$$

For given values of J_a and J_d this quadratic equation generates two roots for n_s: the low density and high density branches, see Fig. 1. For a given value of mass injection rate, two branches merge defining the critical maximal density n_s when the stationary solutions exist; for $n_i > n_s$ no stationary solutions are possible. Similar property was directly observed numerically in [27].

With the value of density from (4), the equation (3a) can be used to find the value of the v_i' by expanding (3a) near the singular point [27]. Thus, the values of v_i', n_i', and ϕ' are found, and the full profiles can be recovered by integration from the sonic point in both directions.

For different combinations of J_a and J_d and parameters from Table 1 values of n_s, v_i', n_i', ϕ' were obtained, and plasma profiles were recovered by the integration from the sonic point in both directions: to the anode and to the cathode. Integration was done by using a 4th order Runge–Kutta method in two directions from $x_s|_{x=0}$ to $x = -L$ and from $x_s|_{x=0}$ to $x = L$, where x_s was set at the sonic point. Integration in negative direction was stopped at the point when ion velocity reached $-c_s$ value; thus, the possible solution is defined on the interval larger than the thruster

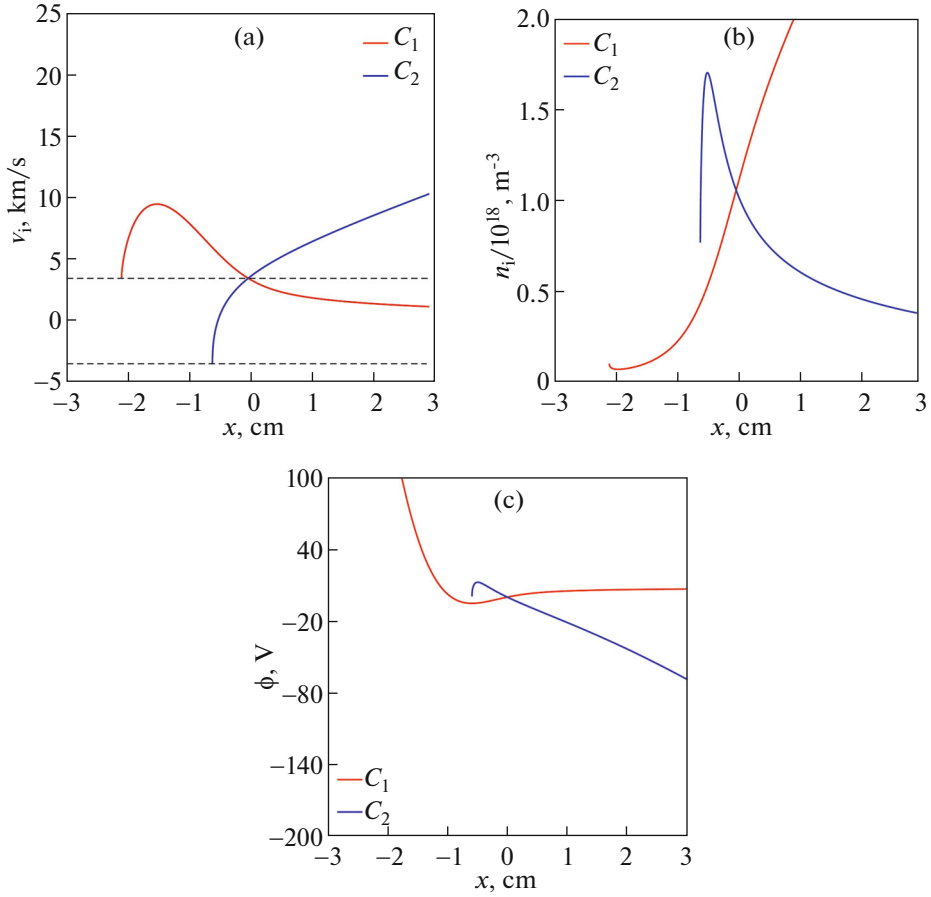

Fig. 2. Profiles of (a) v_i (dashed lines—$\pm c_s$); (b) n_i; and (c) ϕ for root C.

length L. Fixing the system size to the given thruster length L and taking the left boundary value at $v_i = -c_s$ one obtains the value of the potential difference for a given J_d and J_a. Other solutions are possible if one allows values at the anode $|v_i| < c_s$.

However, not all solutions for $n_i < n_s$ are possible: for some values of n_s the corresponding values of the velocity, density, and potential gradients become complex. Solution of Eq. (4) is presented in Fig. 1a as a function of I_d (here $I_d = eJ_dS$), at a fixed value of J_a. For values of the total current smaller than some maximum value, Eq. (4) has two roots, which form high density and low density branches. The real roots for n_s, v_i', n_i', and ϕ' exist only for a certain range of J_a and J_d. It can be seen in Fig. 1b, where velocity gradient as a function of I_d is shown. The real v_i' exists only for the high-density branch of n_s (shown as blue in Fig. 1a) and small region of the low density branch.

Several points were chosen along the n_s curve: A, B, and C to illustrate possible solutions for different values of the discharge current I_d—see Fig. 1a. The corresponding roots for velocity gradients are marked by the same letters on Fig. 1b. For each point on n_s curve there are two reciprocal points on velocity gradient curves.

The root C on n_s curve, corresponding to the high density branch, yields two different real roots for v_i', n_i', and ϕ' yields C_1 and C_2. The profiles of the ion velocity, density, and potential for these roots, obtained by integration, are shown in Fig. 2. As one can see, the C_2 root leads to decelerating solution and is not appropriate for thruster applications. The v_i profile for C_1 root has a region of supersonic ion acceleration with possible c_s value at the anode sheath boundary.

The situation with A and B roots, for the discharge current values close to the maximum, is more complex, as shown in Fig. 3, which is shown not to scale. Part of the diagram in Fig. 1a, marked with red color, corresponds to the n_s range where there are four roots of v_i'. Two roots $B_{1,2}$, corresponding to the point B, have the non-monotonic velocity profiles with two c_s points, which is not possible in case of a pre-sheath region near the anode with the negative ion flow. For the point A, there are two monotonic solutions, an

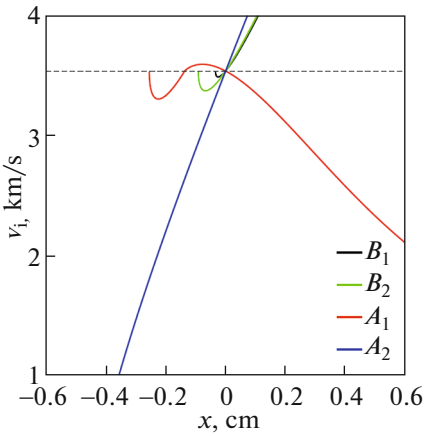

Fig. 3. Velocity profiles for roots A and B; magnified.

only root A_2 produces a profile with supersonic acceleration, which can be matched to the sheath boundary at the anode.

From previous results it is clear that for the given value of the mass flux J_a there exist a range of the discharge currents I_d, where it is possible to find an accelerating solution; however, there exists a range of J_a and I_d values where there are no stationary solutions. The described method allows for obtaining steady-state profiles for various values of operational space parameters, e.g., range of solutions exists with values of the ion velocity at anode $v_i \neq -c_s$ [27].

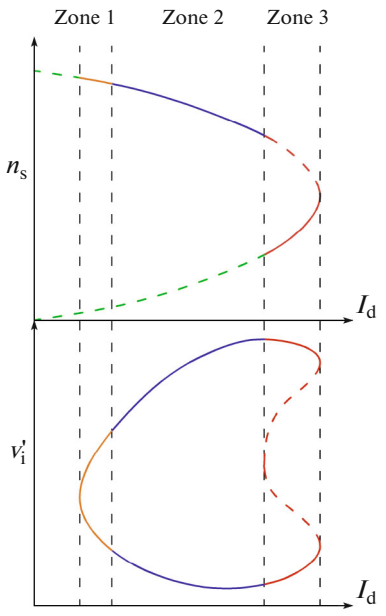

Fig. 4. Stability diagram of stationary solutions in the n_s, v_i', and I_d space at a fixed value of J_a (not in scale). In Zone 1, profiles are stable, there are no oscillations. In Zone 2, there exist strongly coherent oscillations. In Zone 3, the multi-mode oscillations are present. The green dashed part of the diagram correspond to n_s values for which no real values of derivatives v_i', n_i', ϕ_i' exist. For red dashed part of the diagram there are no physically relevant solutions. Parts of the diagram shown by the dashed line in region 3 do not have solutions of physical interest.

4. STABILITY OF STATIONARY SOLUTIONS

We have studied the full time-dependent problem, given by equations (1), using stationary solutions obtained in previous section as an initial state. Initial value problem simulations were performed with BOUT++ framework [36]. Only profiles with Bohm boundary condition ($v_i = -c_s$) at the anode sheath were considered. In this case each profile corresponded to different values of I_d, whilst the value of the mass flow J_a was fixed. Time-dependent simulations were performed for these profiles, used as an initial state (with corresponding BC). The time evolution of the discharge current and characteristic frequency were followed. The main result of these simulations is outlined in the diagram Fig. 4.

It was found that for lower values of the discharge current (in Zone 1, orange solid) the stationary profiles remain stable and there are no current oscillations in this region. The discharge current oscillations appear for profiles from Zone 2. As the value of I_d increases (from left boundary to the right boundary of Zone 2) oscillation frequency and oscillation amplitude started to grow. This is illustrated in Figs. 5a, 5b. However, nature of these oscillations remains the same: the oscillations are purely sinusoidal with one dominant frequency (see Figs. 6a, 6d). At the beginning of Zone 3 frequency and amplitude continue to grow (see Figs. 5a, 5b); however there is a transition to multimode oscillations (see Figs. 6b, 6e). At the end of Zone 3 oscillations amplitude reaches its maximum, but frequency drops abruptly and oscillations become strongly non-linear as in Figs. 6c, 6f.

Figure 5a shows the discharge current (squares) and fluctuations amplitude (triangles) as a function of the discharge voltage, U_D, obtained in the time-dependent simulations. Oscillation frequencies are shown in Fig. 5b. Values of the discharge voltage were found from the stationary solution. As one can see, oscillations of the discharge current grow when roots are getting closer to the maximum possible value of U_D. However, there is a region where there are no oscillations at all. It corresponds to Zone 1 in diagram Fig. 4. This I–V curve has similar features to the experimental diagram (see Fig. 4 in [37]). Comparison between the discharge and ion currents, I_i is shown in Fig. 5c. It is interesting to note that the increase in the discharge current does not result in the corresponding growth of the ion current, which remains almost con-

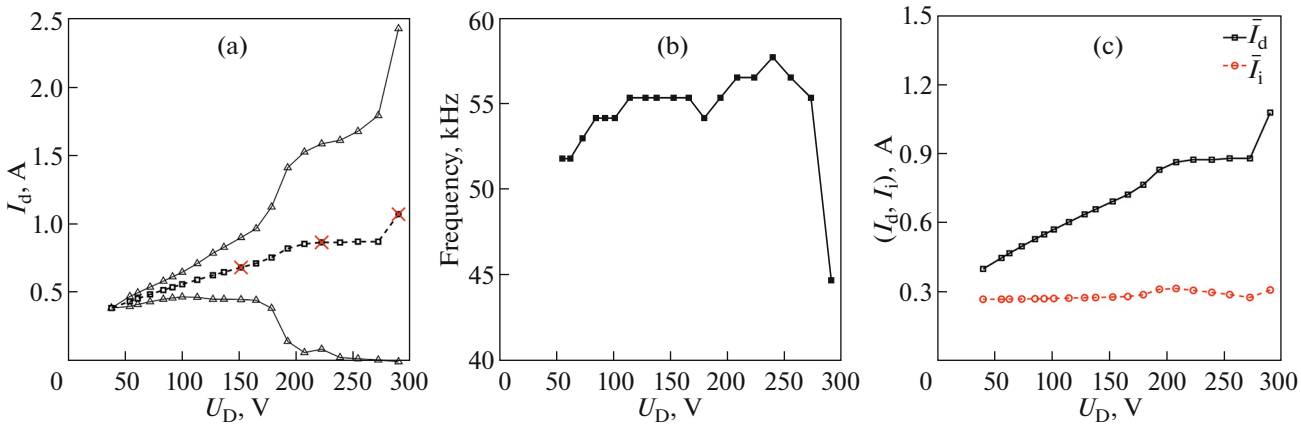

Fig. 5. (a) Extremes of the discharge current fluctuations (triangles) and values of the discharge current (squares) as functions of the discharge voltage. Discharge current traces for points marked with crosses are shown in Fig. 6. (b) Oscillation frequency as a function of the discharge voltage. (c) Discharge (squares) and ion (circles) currents as functions of the discharge voltage. Here and below, the bar symbol corresponds to the time average current value.

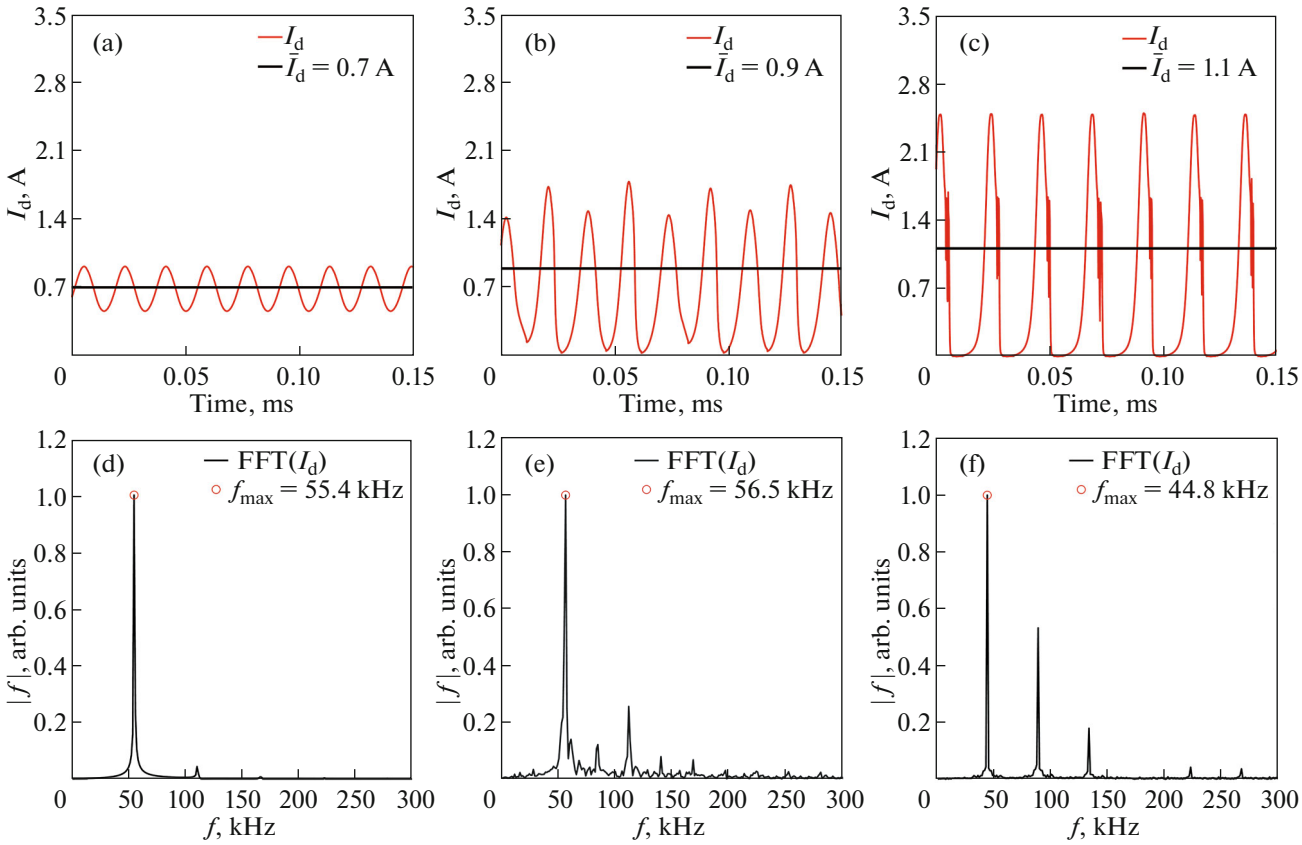

Fig. 6. Discharge current traces (a–c) and corresponding spectra (d–f) for different values of U_D, shown with marks in Fig. 5.

stant. This means that the efficiency of the thruster decreases.

Mode transition, from a single mode oscillations to multi-mode oscillations and then to non-sinusoidal type of oscillation, is shown in Fig. 6. For low values of the discharge current, oscillations are perfectly sinusoidal, see Figs. 6a, 6d, with one dominant mode. When current increases, what corresponds to roots from Zone 3, multimode oscillation appears, see Figs. 6b, 6e. When current is at maximum possible

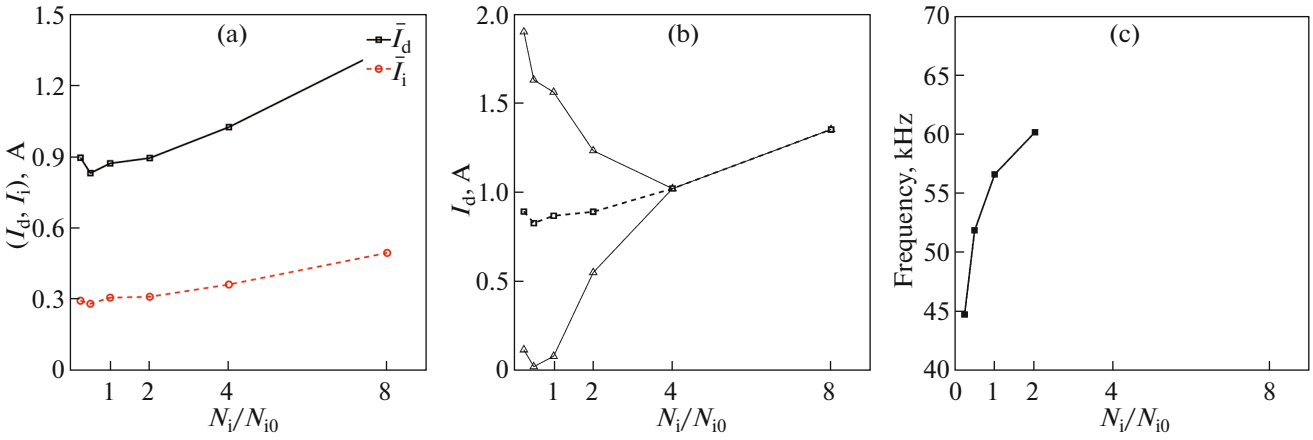

Fig. 7. Effect of plasma density N_i boundary condition at the anode on unstable profile. (a) Values of the discharge and ion currents. (b) Extremes of the discharge current fluctuations (triangles) and values of the discharge current (squares). (c) Oscillation frequency. Here N_{i0} is the value of the density obtained from stationary solutions.

value, oscillations become non-sinusoidal single mode type, see Figs. 6c, 6f.

5. EFFECT OF BOUNDARY CONDITIONS ON THE STABILITY AND OSCILLATIONS CHARACTERISTICS

In this section, the effect of boundary conditions (BC) on the behavior of stationary solutions were studied. In previous section, the same Dirichlet type boundary conditions for plasma density and ion velocity were used as those determined from stationary profiles. The assumption was made, that the "wrong" BC, that are different from those obtained from stationary solutions, may affect oscillations. To investigate this hypothesis, two types of stationary solutions were chosen: stable and unstable (from Zone 1 and Zone 2, respectively); and boundary condition either for the ion velocity or plasma density were changed from the one in the stationary solution, while another condition was kept the same as obtained from stationary solutions.

5.1. Effect of Boundary Conditions on Unstable Profiles

First, unstable profiles were studied with imposed BC on plasma density, while the BC for the ion velocity was kept constant $v_i = -c_s$. Results of time-dependent simulations are shown in Fig. 7. Figures show the discharge and ion currents (Fig. 7a), discharge current oscillations (Fig. 7b), and oscillation frequency (Fig. 7c) as a function of the plasma density at the anode boundary. Plasma density is represented as a ratio of the imposed value N_i to the value found from the stationary solutions N_{i0}. Increase of the plasma density results in the growth of the discharge current, however, changes in the ion current are less significant (see Fig. 7a). Oscillation amplitudes and frequencies are strongly affected by the plasma density at the boundary. Increase of the plasma density at the anode leads to decrease in oscillation amplitude and growth of the oscillation frequency. There is a threshold value, after which oscillations disappear (see Figs. 7b, 7c).

Effect of the ion velocity BC is presented in Fig. 8. Results are shown as functions of the ratio of the imposed ion velocity to the ion sound velocity c_s. Variations of BC at the anode mainly result in changes in oscillation amplitude (see Fig. 8b). There is a change in the discharge and ion current values; however, they are smaller, compare to the case of ion density variations. Frequency of oscillations is weakly affected by ion velocity BC (see Fig. 8c). Interestingly, changes in ion velocity BC do not lead to a suppression of oscillations. In general, the effect of the ion velocity BC is less prominent, compared to the effect of the plasma density.

5.2. Effect of Boundary Conditions on Stable Profiles

Same simulations, as described before, were performed for the case of stable profiles. These profiles do not have intrinsic oscillations, and thus, can be used to verify whether different boundary conditions can cause the system to become unstable.

Effect of plasma density BC is shown in Fig. 9. Similarly to the case of unstable profiles, increase in plasma density leads to the growth of the discharge and ion currents, and this change is almost linear. In this case, ion current changes proportionally to the increase of the discharge current. However, increased ion density BC does not cause destabilization of the system, as can be seen in Fig. 9b, when oscillations are absent for a whole range of imposed density values.

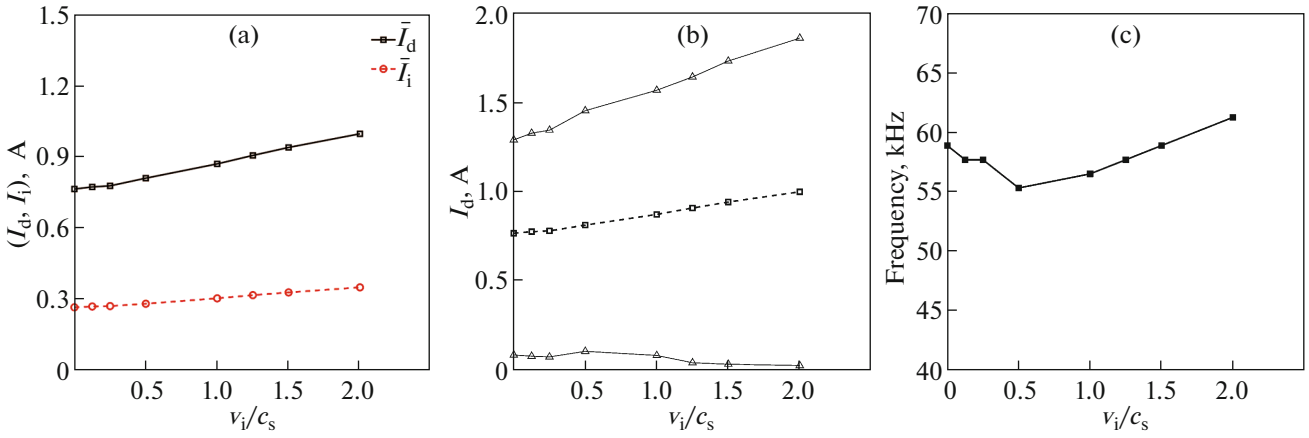

Fig. 8. Effect of ion velocity v_i boundary condition at the anode on unstable profile. (a) The discharge and ion currents. (b) Extremes of the discharge current fluctuations (triangles) and values of the discharge current (squares). (c) Oscillation frequency.

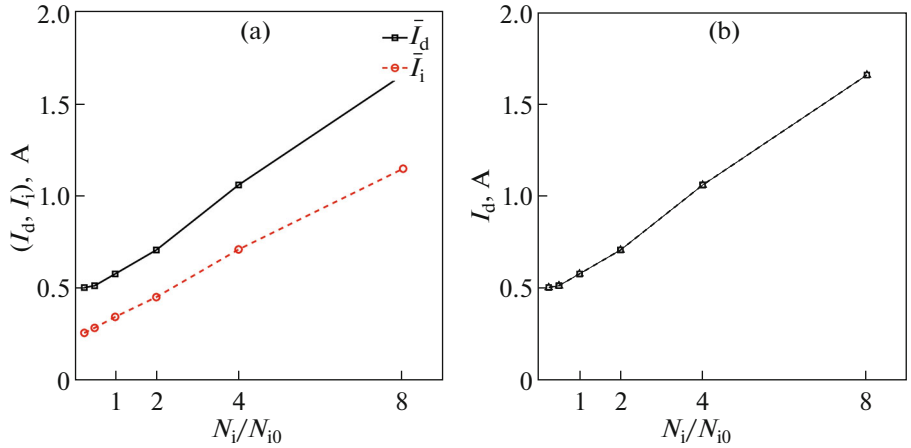

Fig. 9. Effect of plasma density N_i boundary condition at the anode on stable profile. (a) The discharge and ion currents. (b) Extremes of the discharge current fluctuations (triangles) and values of the discharge current (squares). Here, N_{i0} value of the density obtained from stationary solutions.

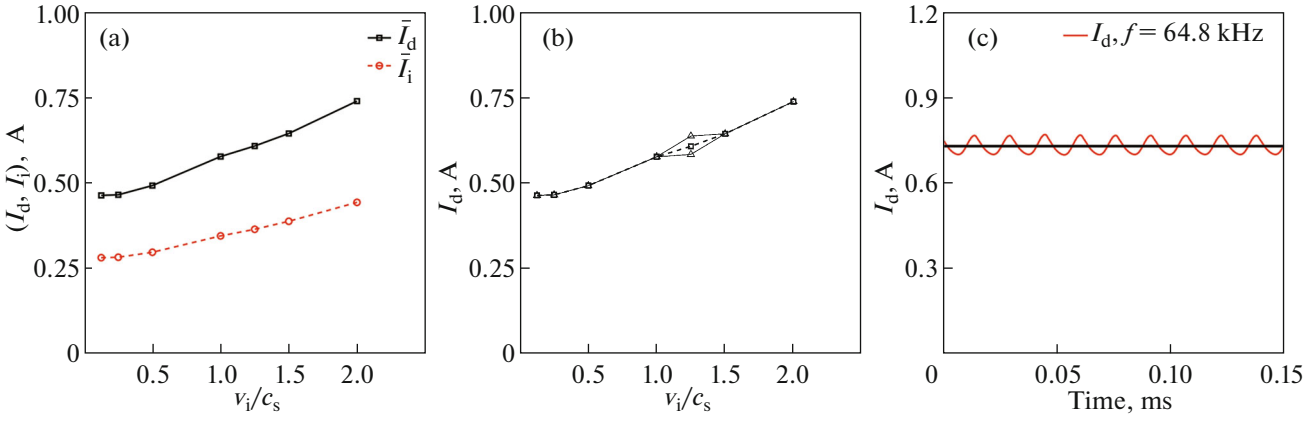

Fig. 10. Effect of ion velocity v_i boundary condition at the anode on a stable profile. (a) The discharge and ion currents. (b) Extremes of the discharge current fluctuations (triangles) and values of the discharge current (squares). (c) The discharge current trace for unstable case.

Changes in ion velocity at the anode boundary lead to a variation of the discharge and ion currents. Same as for unstable profiles, this change is smaller compared to the case of ion density BC variations. However, there is an important difference, as changes in ion velocity can lead to destabilizing the profile. This occurs for a narrow range of ion velocity values, slightly higher than the ion sound velocity. There are single-mode oscillations in the system in this case with frequencies $f \sim 64.8$ kHz, as shown in Fig. 10c.

6. SUMMARY

We have studied the stability properties of the axial ionization mode by using steady-state solutions as an initial state in the time-dependent problem. The time dependent simulations of the system of nonlinear partial differential equations require specification of boundary conditions at the anode. The physics and the exact form of boundary conditions on the anode side of quasineutral region is not completely clear. Assuming existence of the anode sheath, the boundary condition at the boundary of quasineutral region takes the Bohm form $v_i = -c_s$. The zero velocity condition $v_i = 0$ was also used for studies of stationary solutions [38]. It was pointed out that the regimes with modified anode sheath or no sheath are possible in Hall thrusters [30, 39–42], thus opening up possibilities for different boundary conditions. This motivated us to consider the role of modified anode boundary conditions on the mode stability (Fig. 10).

Assuming $v_i = -c_s$ for the ion velocity, boundary condition for the plasma density was obtained self-consistently from the steady-state solution. It was shown that in this case, the operational space diagram is split into three zones. Profiles obtained for the values of the discharge current in Zone 1 are stable and do not have intrinsic oscillations. Profiles in the Zone 2 are unstable with sinusoidal-like single-mode oscillations. Profiles in the Zone 3 are unstable showing strongly nonlinear multi-mode oscillations. This result can be related to the mode transitions, observed experimentally in previous works by Sekerak et al. [43, 44].

To study broader effects of modified boundary conditions, we have considered stability of steady-state profiles allowing for boundary conditions different from those obtained self-consistently for stationary solutions. Profiles from the Zone 1 (stable zone) and Zone 2 (unstable zone) were considered. It was found that for stable profiles (from Zone 1), modification of the density BC does not affect system behavior significantly. There is a linear change in the stationary values of the discharge and ion currents, nonetheless, this does not lead to the excitation of oscillations in the system. Modification of the ion velocity can lead to the destabilization, but in a narrow region. The resulting oscillations are single-mode oscillations with small (compared to the DC level) amplitude, suggesting that the oscillations are in the linear regime [45].

In case of the unstable profiles (Zone 2), modification of the density at the boundary has the strongest effect on the system stability. There exists a threshold level of density for which the oscillations disappear. Increase of the density at the boundary results in the growth of the oscillation frequency as well. Variations of the ion velocity at the boundary have a small effect on the system behavior. There are minor changes in oscillation amplitudes and frequencies, however, the system remains unstable.

Stability of accelerated plasma flow studied in this paper is governed by the interplay of the electron mobility, diffusion, and ionization, which is most similar to the conditions of the breathing mode in Hall thruster. The mobility is anomalous in Hall thrusters; the exact values and the profile of the anomalous mobility (collision frequency) are not so well known [28]. We have used a simplified model with a uniform and constant electron mobility, even though such conditions are not fully realistic for the Hall thrusters, except may be the near anode region. Changing mobility to larger (anomalous) values will result in lower oscillation frequency but it is expected that the general mode behavior and role of boundary conditions will remain similar to our results. We expect that general results of this study will be useful for analysis of the behavior of the breathing mode in experiments for discharge control [46–49] and diagnostic purposes [45, 50], as well as for studies of the regimes with modified anode sheath or no sheath conditions [30, 39].

It is worth noting that axial oscillations of plasma parameters may affect the azimuthal modes driven by density gradients [51, 52], and such a coupling [53] may be different depending on the type of the excited axial modes. It was suggested [54] that the resistive mode instability [55] is crucial for the breathing modes. Such instabilities, excited by the axial electron (resistive) current and the accelerated ion beam [56, 57] are also expected in other systems [1–7].

ACKNOWLEDGMENTS

The authors are grateful to Y. Raitses for many useful discussions.

FUNDING

This work was supported in part by the Russian Science Foundation, Project 17-12-01470.

REFERENCES

1. V. V. Andreev, D. V. Chuprov, V. I. Ilgisonis, A. A. Novitskii, and A. M. Umnov, Phys. Plasmas **24**, 093518 (2017).

2. A. A. Balmashnov, A. V. Kalashnikov, V. V. Kalashnikov, S. P. Stepina, and A. M. Umnov, Plasma Phys. Rep. **44**, 626 (2018).
3. D. Kahnfeld, R. Heidemann, J. Duras, P. Matthias, G. Bandelow, K. Luskow, S. Kemnitz, K. Matyash, and R. Schneider, Plasma Sources Sci. Technol. **27**, 124002 (2018).
4. Y. Yang, X. Zhou, J. X. Liu, and A. Anders, Appl. Phys. Lett. **108**, 034101 (2016).
5. C. V. Young, A. L. Fabris, and M. A. Cappelli, Appl. Phys. Lett. **106**, 044102 (2015).
6. K. V. Brushlinskii and N. S. Zhdanova, Izv. Ross. Akad. Nauk, Mekh. Zhidk. Gaza, No. 3, 135 (2004).
7. K. V. Brushlinskii and N. S. Zhdanova, Plasma Phys. Rep. **34**, 1037 (2008).
8. A. I. Morozov, in *Plasma Accelerators,* Ed. by L. A. Artsimovich, S. D. Grishin, G. L. Grozdovskii, L. V. Leskov, A. I. Morozov, A. M. Dorodnov, V. G. Padalka, and M. I. Pergament (Mashinostroenie, Moscow, 1973), p. 85 [in Russian].
9. A. I. Morozov, Plasma Phys. Rep. **29**, 235 (2003).
10. A. I. Morozov and V. V. Savelyev, in *Reviews of Plasma Physics,* Ed. by B. B. Kadomtsev and V. D. Shafranov (Consultants Bureau, New York, 2000), Vol. 21, p. 203.
11. V. P. Kim, Tech. Phys. **60**, 362 (2015).
12. G. S. Janes, J. Dotson, and T. Wilson, Report No. NP-12154 (Rev.) (AVCO-Everett Research Laboratory, Everett, MA, USA, 1962). https://www.osti.gov/biblio/4715406-electrostatic-acceleration-neutral-plasmas-momentum-transfer-through-magnetic-fields-research-report.
13. J. Fife, M. Martinez-Sanchez, and J. Szabo, in *Proceedings of the 33rd AIAA Joint Propulsion Conference, Seattle, WA, 1997,* Paper AIAA97-3052.
14. J. M. Fife, PhD Thesis (Massachusetts Institute of Technology, Cambridge, MA, USA, 1998).
15. S. Barral and E. Ahedo, AIP Conf. Proc. **993**, 439 (2008)
16. A. I. Morozov, in *Proceedings of the 24th International Electric Propulsion Conference, Moscow, 1995,* Paper IEPC-95-161.
17. A. I. Morozov and V. V. Savelyev, Plasma Phys. Rep. **26**, 875 (2000).
18. S. Barral, Z. Peradzynski, K. Makowski, and M. Dudeck, High Temp. Mater. Processes: Int. Q. High-Technol. Plasma Processes **5** (2), 2001. https://doi.org/10.1615/HighTempMatProc.v5.i2.100
19. J. P. Boeuf and L. Garrigues, J. Appl. Phys. **84**, 3541 (1998).
20. S. Barral and E. Ahedo, Phys. Rev. E **79**, 046401 (2009).
21. N. Yamamoto, T. Nakagawa, K. Komurasaki, and Y. Arakawa, Vacuum **65**, 375 (2002).
22. K. Hara, M. J. Sekerak, I. D. Boyd, and A. D. Gallimore, Phys. Plasmas **21**, 122103 (2014).
23. L. Q. Wei, L. Han, D. R. Yu, and N. Guo, Chin. Phys. B **24**, 055201 (2015).
24. N. J. Fisch and A. Fruchtman, Modeling the Hall thruster, PPPL rep. 8, 1998.
25. A. Fruchtman, N. J. Fisch, and Y. Raitses, Phys. Plasmas **8**, 1048 (2001).
26. E. Ahedo, J. M. Gallardo, and M. Martinez-Sanchez, Phys. Plasmas **9**, 4061 (2002).
27. A. Smolyakov, O. Chapurin, I. Romadanov, Y. Raitses, and I. Kaganovich, AIAA Propulsion and Energy Forum, AIAA 2019-4080 (2019). https://doi.org/10.2514/6.2019-4080
28. I. G. Mikellides and A. L. Ortega, Plasma Sources Sci. Technol. **28**, 014003 (2019).
29. J. P. Boeuf, Phys. Plasmas **26**, 072113 (2019).
30. L. Dorf, V. Semenov, and Y. Raitses, Appl. Phys. Lett. **83**, 2551 (2003).
31. A. Fruchtman, N. J. Fisch, and Y. Raitses, Phys. Plasmas **8**, 1048 (2001).
32. A. Smirnov, Y. Raitses, and N. J. Fisch, IEEE Trans. Plasma Sci. **36**, 1998 (2008).
33. A. Smirnov, Y. Raitses, and N. J. Fisch, Phys. Plasmas **14**, 057106 (2007).
34. A. Smirnov, Y. Raitses, and N. J. Fisch, J. Appl. Phys. **92**, 5673 (2002).
35. N. J. Fisch and A. Fruchtman, in *Proceedings of the 34st AIAA/ASME/SAE/ASEE Joint Propulsion Conference and Exhibit, Cleveland, USA, 1998,* Paper AIAA98-3500.
36. B. D. Dudson, A. Allen, G. Breyiannis, E. Brugger, J. Buchanan, L. Easy, S. Farley, I. Joseph, M. Kim, A. D. McGann, J. T. Omotani, M. V. Umansky, N. R. Walkden, T. Xia, and X. Q. Xu, J. Plasma Phys. **81**, 365810104 (2015).
37. N. Gascon, M. Dudeck, and S. Barral, Phys. Plasmas **10**, 4123 (2003).
38. A. Cohen-Zur, A. Fruchtman, J. Ashkenazy, and A. Gany, Phys. Plasmas **9**, 4363 (2002).
39. E. Ahedo and J. Rus, J. Appl. Phys. **98**, 043306 (2005).
40. L. Dorf, Y. Raitses, and N. J. Fisch, Phys. Plasmas **13**, 057104 (2006).
41. L. Dorf, Y. Raitses, and N. J. Fisch, J. Appl. Phys. **97**, 103309 (2005).
42. M. Keidar, J. Appl. Phys. **103**, 053309 (2008).
43. M. J. Sekerak, R. Hofer, J. Polk, B. Longmier, A. Gallimore, and D. Brown, in *Proceedings of the 49th AIAA/ASME/SAE/ASEE Joint Propulsion Conference and Exhibit, San Jose, CA, USA, 2013,* Paper AIAA13-5468.
44. K. Hara, M. J. Sekerak, I. D. Boyd, and A. D. Gallimore, J. Appl. Phys. **115**, 203304 (2014).
45. I. Romadanov, Y. Raitses, and A. Smolyakov, Plasma Sources Sci. Technol. **27**, 094006 (2018).
46. T. Furukawa, T. Miyasaka, and T. Fujiwara, Trans. Jpn. Soc. Aeronaut. Space Sci. **44**, 164 (2001).
47. D. R. Yu, C. S. Wang, L. Q. Wei, C. Gao, and G. Yu, Phys. Plasmas **15**, 113503 (2008).
48. C. Wang, L. Wei, and D. Yu, Contrib. Plasma Phys. **51**, 981 (2011).

49. L. Q. Wei, K. Han, C. S. Wang, H. Li, C. H. Zhang, and D. R. Yu, J. Vac. Sci. Technol., A **30**, 061304 (2012).
50. I. Romadanov, Y. Raitses, A. Diallo, K. Hara, I. D. Kaganovich, and A. I. Smolyakov, Phys. Plasmas **25**, 033501 (2018).
51. I. Romadanov, A. Smolyakov, Y. Raitses, I. Kaganovich, T. Tian, and S. Ryzhkov, Phys. Plasmas **23**, 122111 (2016).
52. A. I. Smolyakov, O. Chapurin, W. Frias, O. Koshkarov, I. Romadanov, T. Tang, M. Umansky, Y. Raitses, I. D. Kaganovich, and V. P. Lakhin, Plasma Phys. Controlled Fusion **29**, 014041 (2017).
53. I. Romadanov, E. Raitses, and A. Smolyakov, Plasma Phys. Rep. **45**, 134 (2019).
54. S. Chable and F. Rogier, Phys. Plasmas **12**, 033504 (2005).
55. O. Koshkarov, A. I. Smolyakov, A. Kapulkin, Y. Raitses, and I. Kaganovich, Phys. Plasmas **25**, 061209 (2018).
56. O. Koshkarov, A. I. Smolyakov, I. V. Romadanov, O. Chapurin, M. V. Umansky, Y. Raitses, and I. D. Kaganovich, Phys. Plasmas **25**, 011604 (2018).
57. O. Koshkarov, A. I. Smolyakov, I. D. Kaganovich, and V. I. Ilgisonis, Phys. Plasmas **22**, 052113 (2015).